Laser-induced electron dynamics including photoionization: A heuristic model within time-dependent configuration interaction theory

Stefan Klinkusch, Peter Saalfrank, and Tillmann Klamroth[a)]
Institut für Chemie, Universität Potsdam, Karl-Liebknecht-Str. 24-25, D-14476 Potsdam-Golm, Germany

(Received 24 June 2009; accepted 14 August 2009; published online 16 September 2009)

We report simulations of laser-pulse driven many-electron dynamics by means of a simple, heuristic extension of the time-dependent configuration interaction singles (TD-CIS) approach. The extension allows for the treatment of ionizing states as nonstationary states with a finite, energy-dependent lifetime to account for above-threshold ionization losses in laser-driven many-electron dynamics. The extended TD-CIS method is applied to the following specific examples: (i) state-to-state transitions in the LiCN molecule which correspond to intramolecular charge transfer, (ii) creation of electronic wave packets in LiCN including wave packet analysis by pump-probe spectroscopy, and, finally, (iii) the effect of ionization on the dynamic polarizability of H_2 when calculated nonperturbatively by TD-CIS. © *2009 American Institute of Physics*. [doi:10.1063/1.3218847]

I. INTRODUCTION

Experimentally, laser-driven electron dynamics on ultrashort, possibly attosecond (1 as$=10^{-18}$ s) time scales is currently being extended from the atomic[1] to the molecular world.[2–4] As far as theory is concerned, the numerically exact solution of the nonrelativistic, electronic Schrödinger equation in real time has been achieved for the simplest molecules only such as H_2^+ or H_2.[5] (For these, also nuclear motion can be included.[6,7]) Therefore, efficient correlated many-electron methods are required which can be applied to larger molecular systems.

One such method is explicitly time-dependent density functional theory.[8] The method is correlated and efficient; however, there are also problems when treating Rydberg states, dispersion forces, or long-range charge transfer.[9] A useful alternative is time-dependent configuration interaction (TD-CI) method. The simplest variant is time-dependent configuration interaction singles (TD-CIS) which contains single excitations only.[10–12] TD-CIS is systematically improvable toward the full-CI limit by including double, triple,… excitations either exactly (TD-CISD,[12,13] TD-CISDT,…) or perturbatively [for instance in TD-CIS(D) (Ref. 14)]. The TD-CI method can be viewed as a special variant of the more general explicitly time-dependent complete active space self consistent field (CASSCF) approach, also known as multiconfigurational time-dependent Hartree–Fock), in which both the configurations and their coefficients are explicitly time dependent.[15–17] Also other time-dependent CI-type expansions of the many-electron wave function are known and in use[18,19] for interesting dynamical phenomena such as ring currents[19] or charge migration.[18]

Our own applications of TD-CI for laser-driven electron dynamics in molecules range from state-to-state transitions including intramolecular[14,20] and long-range intermolecular charge transfer,[21,22] over the creation of electronic wave packets[14,21] and the nonperturbative calculation of molecular response properties,[14] to the extension of the method to dissipative media.[23] In these applications, and in many of those cited above atom-centered Gaussian basis sets have been used. This means that large-amplitude electron motion, ionization losses, and energy-resolved photoelectron spectroscopies cannot be treated. To allow for that, grid or plane-wave-type bases or basis functions with special boundary conditions are needed. In the context of TD-CI or related methods, unbound electron motion on grids has so far been realized for low-dimensional (typically one-dimensional) model systems only.[10,11,15,17,24,25] For real molecules ionization is hardly ever included except for the simplest one- or two-electron species.[5–7] It is the goal of this paper to devise a simple, heuristic model by which ionization processes in molecules and related phenomena can be included in an approximate fashion.

Let us recall that there are two different types of photoionization. One is below-threshold ionization,[26–28] where electrons tunnel through the barrier which changes periodically with the field oscillations. Tunnel ionization occurs mainly when the excitation frequency is below the ionization potential (IP), and if field intensities are so low that multiphoton excitation is suppressed. At sufficiently high frequencies, and/or at high intensities, on the other hand, above-threshold ionization is dominant. Note, however, that for very high intensities even for frequencies above the IP, tunnel ionization may become more and more important. The relevance of tunnel ionization can be determined by calculating the Keldysh[26] factor γ,

$$\gamma = \sqrt{\frac{\mathrm{IP}}{2U_P}}, \tag{1}$$

where IP is the ionization potential of the system and U_P is the ponderomotive energy calculated from the maximal electric field $|\underline{F}_{\max}|$ and the frequency ω according to

[a)]Electronic mail: klamroth@rz.uni-potsdam.de.

$$U_P = \frac{|\underline{F}_{\max}|^2}{4\omega^2}. \tag{2}$$

If the Keldysh parameter is $\gamma \ll 1$, tunnel ionization is dominant.

The model to be described in more detail below is derived for the above-threshold scheme. This is done by interpreting those CIS eigenstates with energies above the ionization threshold as nonstationary, having a lifetime given by the inverse of its ionization rate. The approach is similar to a complex absorbing potential[29] in energy space. As a consequence, ionization losses including time-resolved photoelectron spectra can be described but large-amplitude motions such as recollisions during high-order harmonic generation,[30] or tunneling/diffraction processes,[31] are not captured by this model.

The paper is organized as follows. In Sec. II, we sketch the TD-CIS approach and its extension containing absorbing boundaries. In Sec. III, results for state-to-state-excitations below or above the ionization threshold are presented for a LiCN molecule as a first example. In Sec. IV, the creation of an electronic wave packet is demonstrated for the same molecule. The wave packet motion is monitored by a time-resolved ionization yield obtained from pump-probe techniques. Finally, in Sec. V we show how photoionization may affect the response properties of molecules when stimulated with laser pulses. This will be demonstrated for the example of the dynamic polarizability of a H_2 molecule. Section VI summarizes the paper. Unless stated otherwise, all quantities in this work will be given in atomic units ($\hbar = m_e = 4\pi\epsilon_0 = e = 1$), but $\hbar$ and e will often be indicated for clarity.

II. THEORY

A. The TD-CIS method

Let us briefly recall the essential features of the TD-CIS method. We solve the time-dependent electronic Schrödinger equation within the semiclassical dipole approximation

$$i\frac{\partial \Psi(t)}{\partial t} = [\hat{H}_0 - \hat{\underline{\mu}}\underline{F}(t)]\Psi(t). \tag{3}$$

The field-free electronic Hamiltonian $\hat{H}_0$ within the fixed nuclei approximation for a molecule consisting of N electrons and N_A nuclei is given as

$$\hat{H}_0 = -\frac{1}{2}\sum_{i=1}^{N}\Delta_i + \sum_{i=1}^{N}\sum_{j>i}^{N}\frac{1}{r_{ij}} - \sum_{A=1}^{N_A}\sum_{i=1}^{N}\frac{Z_A}{r_{iA}}, \tag{4}$$

where $r_{ij} = |\underline{r}_i - \underline{r}_j|$ and $r_{iA} = |\underline{r}_i - \underline{r}_A|$ are interelectronic and electron-nuclei distances, respectively. Z_A is the charge of nucleus A, $\hat{\underline{\mu}} = -\Sigma_{i=1}^{N}\underline{r}_i + \Sigma_{A=1}^{N_A} Z_A \underline{R}_A$ is the dipole operator, and $\underline{F}(t)$ is the laser field. The time-dependent wave function within the TD-CIS method is a linear combination of eigenstate functions Ψ_n^{CIS} with energies E_n^{CIS},

$$\Psi(t) = \sum_n C_n(t)\Psi_n^{\mathrm{CIS}}, \tag{5}$$

with the coefficients squared giving the population in state n, i.e., $P_n(t) = |C_n(t)|^2$. As usual, the coefficients can be obtained from

$$i\frac{dC_n(t)}{dt} = \sum_m C_m(t)(V_{nm}(t) + E_n^{\mathrm{CIS}}\delta_{nm}), \tag{6}$$

where

$$V_{nm}(t) = -\underline{\mu}_{nm}\underline{F}(t) \tag{7}$$

are the molecule-field coupling elements which contain the transition dipole matrix elements $\underline{\mu}_{nm} = \langle \Psi_n^{\mathrm{CIS}} | \hat{\underline{\mu}} | \Psi_m^{\mathrm{CIS}} \rangle$. Further, we consider optical transitions between singlet states only given as

$$\Psi_n^{\mathrm{CIS}} = D_{0,n}\Psi_0^{\mathrm{HF}} + \sum_a \sum_r D_{a,n}^r \, {}^1\Psi_a^r. \tag{8}$$

Here, Ψ_0^{HF} is the Hartree–Fock ground state Slater determinant and ${}^1\Psi_a^r = 1/\sqrt{2}(\Psi_a^r + \Psi_{\bar{a}}^{\bar{r}})$ are singlet configuration state functions (CSFs) (Ref. 32) arising from exciting an $\alpha(\Psi_a^r)$ or a $\beta(\Psi_{\bar{a}}^{\bar{r}})$ electron from the occupied spatial orbital a to the virtual orbital r. The inner coefficient vectors $\underline{D}_n = (D_{0,n}; \{D_{a,n}^r\})$ and CIS energies E_n^{CIS} are obtained from the secular equation

$$\underline{\underline{H}}^{\mathrm{CIS}}\underline{D}_i = E_i^{\mathrm{CIS}}\underline{D}_i. \tag{9}$$

$\underline{\underline{H}}^{\mathrm{CIS}}$ is the matrix representation of the field-free Hamiltonian $\hat{H}_0$ in the basis of the ground and singly excited CSFs Ψ_0^{HF} and ${}^1\Psi_a^r$. According to Brillouin's theorem,[33] the ground state is the Hartree–Fock ground state, i.e., $E_0^{\mathrm{CIS}} = E_0^{\mathrm{HF}}$. For the numerical propagation of the outer coefficients an operator splitting technique is used[10] with

$$\underline{C}(t + \Delta t) = \left[\prod_{q=x,y,z} \underline{\underline{U}}_q^{\dagger} e^{iF_q(t)\underline{\underline{\mu}}_q \Delta t}\underline{\underline{U}}_q\right] e^{-i\underline{\underline{H}}\Delta t}\underline{C}(t). \tag{10}$$

In Eq. (10), $\underline{\underline{H}}$ is the field-free Hamiltonian matrix in the basis of the CIS eigenstates, i.e., a diagonal matrix with $H_{nm} = E_n^{\mathrm{CIS}}\delta_{nm}$. Further, $\underline{\underline{U}}_q$ is a unitary matrix transforming the wave function from the CI eigenstate basis into a basis where the dipole matrix $\underline{\underline{\mu}}_q$ is diagonal. F_q is the corresponding electric field component along coordinate q. Equation (10) is only used when the laser field is on. Otherwise the unitary transformation is omitted. Typically, all singlet CIS states within the given basis are included in the calculation.

B. A heuristic model for the inclusion of ionization

In typical CIS calculations with localized basis functions most of the CI states are above the molecular IP, and thus merely discrete representations of continuum states or resonances. On the other hand, even for valence excitations below IP short intense pulses can lead via multiphoton processes to (temporary) population of ionizing states.

Above-threshold ionization is treated in the following by simply replacing every state energy E_n^{CIS} in Eq. (6) by a complex energy

$$E_n^{\mathrm{CIS}} \to E_n^{\mathrm{CIS}} - \frac{i}{2}\Gamma_n, \tag{11}$$

or, equivalently, by extending Eq. (10) as

$$\underline{C}(t+\Delta t) = \left[\prod_{q=x,y,z} \underline{\underline{U}}_q^{\dagger} e^{iF_q(t)\underline{\underline{\mu}}_q \Delta t} \underline{\underline{U}}_q\right] e^{-i\underline{\underline{H}}\Delta t} e^{(-1/2)\underline{\underline{\Gamma}}\Delta t} \underline{C}(t), \tag{12}$$

where $\underline{\underline{\Gamma}}$ is a diagonal matrix containing the Γ_n, $\Gamma_{nm}=\Gamma_n\delta_{nm}$. Γ_n is the ionization rate of CIS state n and $(-i/2)\Gamma_n$ can be interpreted as an absorbing potential for state n, which irreversibly depopulates that state with a lifetime $\tau_n=1/\Gamma_n$.

While for tunneling ionization rates, which are not explicitly considered here, approximate theories have been developed such as the Ammosov–Delone–Krainov model[28] or perturbation theory;[34] this is not the case for the above-threshold limit. For above-threshold ionization we use a simple heuristic model instead. A requirement for the model is that the ionization rate should increase with the excited CIS state energy. However, there may also be "stability islands" if core excitations $a \to r$ took place, for which the total energy may be high but the final orbital with energy ε_r is still bound. In a strict one-electron picture, an electron in an orbital r with a positive energy ε_r has, classically, the kinetic energy $\varepsilon_r=\frac{1}{2}v^2$, where v is the escape velocity of the electron. Thus one has $v=\sqrt{2\varepsilon_r}=\tilde{d}/\tau$, where $\tilde{d}$ is a characteristic escape length which the electron can travel during the time interval τ. Interpreting τ as the lifetime (inverse ionization rate) of the one-electron system, we thus have $\Gamma=1/\tilde{d}\sqrt{2\varepsilon_r}$. Based on this argument, we define the ionization rate of CIS state n of an N-electron system as

$$\Gamma_n = \begin{cases} 0 & \text{if } E_n^{\mathrm{CIS}} < \mathrm{IP} \\ \sum_a \sum_r |D_{a,n}^r|^2 \frac{1}{d}\sqrt{\varepsilon_r} & \text{if } E_n^{\mathrm{CIS}} \geq \mathrm{IP} \text{ and } \varepsilon_r > 0. \end{cases} \tag{13}$$

Here, $|D_{a,n}^r|^2$ is the probability that an excitation from orbital a to orbital r took place in the nth CIS state Ψ_n^{CIS}, and $1/d=\sqrt{2}/\tilde{d}$ is the inverse of the escape length in which the factor $\sqrt{2}$ has been absorbed for convenience. For Eq. (13) we calculate IP in the spirit of the one-electron picture according to Koopmans' theorem as $-\varepsilon_H$, where ε_H is the (Hartree–Fock) orbital energy of the highest occupied molecular orbital (MO) of the molecule.[35] Further, we request that only orbitals with positive ε_r can ionize, i.e., if $\varepsilon_r<0$ the corresponding CSF has no contribution to the ionization rate according to Eq. (13). Further, all states with energies E_n^{CIS} below the ionization threshold do not ionize. The choice of the escape length d in Eq. (13), i.e., the distance after which a (classical) electron can be considered as "free," is somewhat arbitrary and will be motivated below.

C. Laser pulses

In this work, we use $\cos^2$-shaped laser pulses for which the time-dependent electric field is given as

$$\underline{F}(t) = \underline{f}(t)\cos[\omega(t-t_p)], \tag{14}$$

$$\underline{f}(t) = \begin{cases} \underline{f}_0 \cos^2\left[\frac{\pi}{2\sigma}(t-t_p)\right] & \text{if } |t-t_p| < \sigma \\ \underline{0} & \text{else.} \end{cases} \tag{15}$$

At time t_p the pulse is maximal, σ is the full width at half maximum, and 2σ is the total pulse length. $\underline{f}_0$ is the field at $t=t_p$. In most cases single π-pulses or sequences of π-pulses are used. π-pulses lead to population inversion in ideal two-level systems within the rotating wave approximation (RWA).[36] If the transition dipole moment $\underline{\mu}_{fi}$ connecting initial state $|i\rangle$ with final state $|f\rangle$ and $\underline{f}_0$ are parallel to each other, the π-pulse condition is

$$|\underline{\mu}_{fi}||\underline{f}_0|\sigma = \pi. \tag{16}$$

Further, the laser frequency must be resonant at $\omega_{fi}=(E_f^{\mathrm{CIS}}-E_i^{\mathrm{CIS}})/\hbar$. If wave packets are being created or dynamic polarizabilities are determined instead, non-π pulses will be used below.

III. STATE-TO-STATE TRANSITIONS IN LiCN

A. Above-threshold ionization rates for LiCN

1. CIS calculations for LiCN

As a first example, the linear LiCN molecule (Li–C bond along z-axis) is investigated. The molecule was already studied with TD-CIS(D) without ionization in Ref. 14 and in the context of dissipative electron dynamics in Ref. 23. Here we include ionization as described above by means of the modified TD-CIS method. The molecular geometry was optimized at the restricted Hartree-Fock (RHF)/6-31G* level[37] with the GAUSSIAN program package.[38] The optimal bond lengths are $r_{\mathrm{LiC}}=3.68a_0$ (1.95 Å) and $r_{\mathrm{CN}}=2.17a_0$ (1.15 Å), respectively.

In this geometry, a RHF/6-31 G* single point calculation with the GAMESS package[39] was performed and one- and two-electron integrals, MO energies, and MOs taken for use in a CIS calculation. For all 186 singlet CIS state energies, dipole moments and transition dipole moments were determined. The lowest 18 of these, S_0 to S_{17}, are below the ionization potential of IP=0.390 79E_h and are shown in Fig. 1. Note that the energies slightly differ from those of Refs. 14 and 23, where CIS(D) was used instead of CIS. The singlet ground state S_0, which defines our energy zero, corresponds to an ionic state with the formal charge distribution $\mathrm{Li}^+\mathrm{CN}^-$ and a large, negative dipole moment $\mu_{00,z}=-3.708ea_0$ pointing along the molecular axis from the CN end to Li. ($\mu_{ij,q}$ denotes the q-component of the (i,j) element of the dipole matrix.) States S_2 and S_3 are degenerate ($E_{2,3}^{\mathrm{CIS}}=0.241\,802E_h$), intramolecular charge transfer states with formal charge distribution $\mathrm{Li}^0\mathrm{CN}^0$, and an inverted dipole moment of $\mu_{22,z}=\mu_{33,z}=+2.795ea_0$. State S_9 is a nondegenerate state ($E_9^{\mathrm{CIS}}=0.302\,778E_h$) with an intermediate dipole moment $\mu_{99,z}=1.234ea_0$. States S_0 and S_2 are connected by a nonvanishing, dominantly x-polarized transition dipole moment of $\mu_{02,x}=0.3082ea_0$. States S_2 and S_9 are connected by a larger transition dipole moment of $\mu_{29,x}=-1.6019ea_0$ with the same polarization. 168 CIS states are above IP and can ionize according to our model. The highest state S_{185} has an energy of 5.252 638E_h.

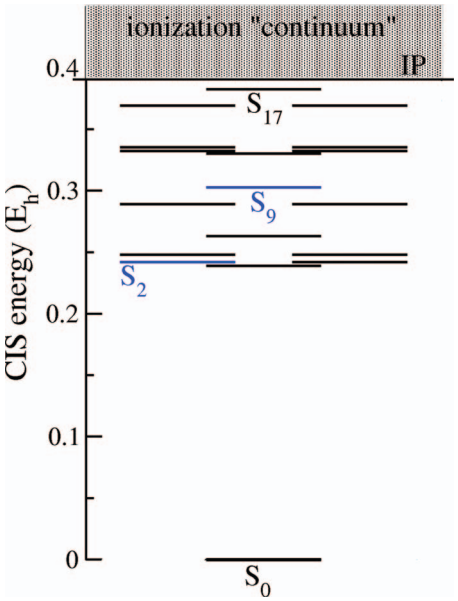

FIG. 1. CIS/6-31G* eigenstates for the linear LiCN molecule up to IP $=0.390\,79E_h$ as calculated from Koopmans' theorem.

2. Escape parameter d and ionization rates

To treat the above-threshold ionization using the simple model of above, the length parameter d in Eq. (13) must be determined. For this purpose we calculate the ionization probability as the total loss of norm $1-\Sigma_n P_n$ during an excitation/deexcitation event. Specifically we consider a sequence of four nonoverlapping π-pulses tailored to enforce the transitions

$$S_0 \rightarrow S_2 \rightarrow S_9 \rightarrow S_2 \rightarrow S_0. \tag{17}$$

The first pulse is x-polarized (i.e., perpendicular to the molecular axis) with pulse parameters $t_p=2000\hbar/E_h$ (48.4 fs, 1 fs$=10^{-15}$ s), $\sigma=2000\hbar/E_h$ (48.4 fs), $\omega=0.2418E_h/\hbar$, and $f_0=0.0051E_h/ea_0$. The second one is also x-polarized with $t_p=6000\hbar/E_h$ (145.1 fs), $\sigma=2000\hbar/E_h$ (48.4 fs), $\omega=0.0610E_h/\hbar$, and $f_0=0.0010E_h/ea_0$. The deexcitations to S_2 and then to S_0 are performed with the same two pulses in reverse order, starting at $t=8000\hbar/E_h$ (193.5 fs) and $t=12\,000\hbar/E_h$ (290.3 fs), respectively. The entire sequence ends after $t=16\,000\hbar/E_h$ (387.0 fs). For the first and last pulses, the maximal field intensity is 9.12×10^{13} and 3.51×10^{10} W/cm^2 for the second and third pulses. At least for the first and fourth pulses, multiphoton transitions cannot be neglected. Also, the deexcitation sequence $S_9\rightarrow S_2\rightarrow S_0$ can be accompanied by absorption to higher, possibly ionizing, states. As a consequence, there will be a loss of norm. After a final propagation time $t_{\mathrm{end}}=26\,000\hbar/E_h$ (628.9 fs) the norm does not change anymore. Various calculations were carried out with different length parameters d. The result is shown in Fig. 2.

From this figure, one can see that the loss of norm becomes maximal with a value of about 0.13 at $1/d\approx1a_0^{-1}$. If the escape length d is very large (i.e., $1/d$ small), then no ionization occurs because the (classical) electron has to travel too far to be counted as free. On the other hand, for very small d (i.e., if $1/d$ is large), the ionization probability

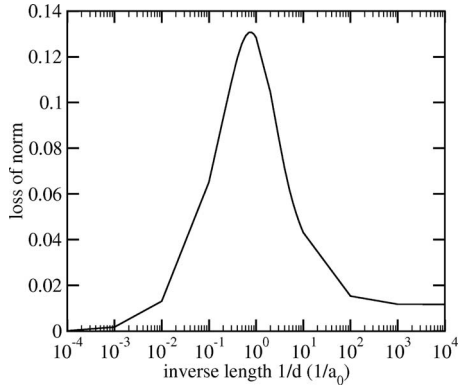

FIG. 2. Loss of norm during a π-pulse sequence in the LiCN system for different length parameters d (see text for details).

is also low. This can be rationalized as follows. For absorbing potentials in real space two sources of error are the transmission through or the reflection from the absorbing potential.[29] However, it should be noted that the analogy to an absorbing potential is not completely fair, as the absorber used here is diagonal in energy space and an absorbing potential in real space. Nevertheless, one can see that for large $1/d$ values the "absorbing potentials" $(-i/2)\Gamma_n$ defined by Eq. (13) are unphysically large, such that the transient population of higher excited states is "reflected" back to stable, below-threshold states before ionization took place. Note that the reflection is incomplete, i.e., a rest population remains above threshold and is eventually ionized. At the maximum of Fig. 2 at $1/d\approx1a_0^{-1}$, the ionization rate may well be overestimated because a (classical) electron traveling a distance $d\approx1a_0$ is already counted as free. Nevertheless, in the following we will adopt the value $1/d=1a_0^{-1}$ throughout to study a *worst* case scenario, or in other words, a situation with an upper bound for the ionization probability.

Within this simplified model and the choice $d=1a_0$, the ionization rates for all states S_n of LiCN were computed (see Fig. 3, upper panel). Below IP, all rates are zero by definition. Above IP, the rates increase with increasing energy as expected. The typical ionization rates Γ_n in this regime are in

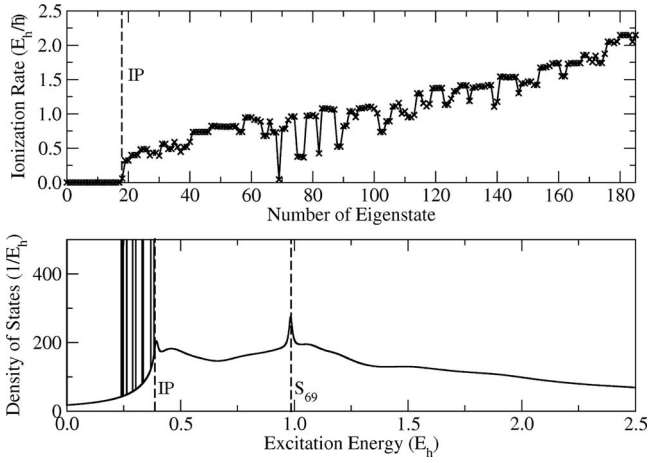

FIG. 3. Upper panel: ionization rates Γ_n for all CIS/6-31G* eigenstates of the LiCN molecule with the choice $d=1a_0$. In the lower panel, the density of states according to Eq. (18) is plotted. The discrete states for $E_n^{\mathrm{CIS}}<\mathrm{IP}$ are indicated by vertical lines representing delta functions.

the order of $1E_h/\hbar$, which corresponds to extremely short lifetimes τ_n of $1\hbar/E_h$, or about 24 as. Note that according to Fig. 3, the increase in Γ_n with n is not monotonic, however, but rather shows stability islands as required above. For example, states S_{18} ($E_{18}^{\mathrm{CIS}}=0.392\,30E_h$) and S_{69} ($E_{69}^{\mathrm{CIS}}=0.983\,49E_h$) are comparatively "long lived" with $\tau_{18}=17\hbar/E_h$ (about 0.4 fs) and $\tau_{69}=22\hbar/E_h$ (about 0.5 fs), respectively. S_{69} has a relatively low ionization rate because the CSF with the largest coefficient $D_{4,69}^{9}=-0.673\,632$ is related to the excitation of an electron from MO 4 (the first non-1s orbital) to the lowest unoccupied molecular orbital (MO 9) with energy $\varepsilon_9=-0.0141E_h$. This is a high-energy excitation; however, the final orbital has an energy $\varepsilon_r<0$ and thus cannot contribute to Γ_{69} according to Eq. (13).

The finite lifetimes of above-threshold states give rise to broadening effects, which can be visualized by the density of states $\rho(E)$, defined as a sum of normalized Lorentzians of width Γ_n each,

$$\rho(E)=\frac{1}{\pi}\sum_n \frac{\Gamma_n/2}{(E-E_n^{\mathrm{CIS}})^2+\left(\frac{\Gamma_n}{2}\right)^2}. \tag{18}$$

As one can see from the lower panel of Fig. 3 where $\rho(E)$ is plotted, we obtain narrow peaks (delta functions) for all states below IP. In contrast the states above the ionization threshold merge into a broad, structureless continuum. An exception where the Lorentzian is still resolved is state S_{69}, for which FWHM$=\Gamma_{69}=0.044\,572E_h$ ($\sim$1.2 eV).

B. Transitions to nonionizing states

We now investigate how photoionization affects state-to-state transitions to nonionizing states. The example we choose is the sequence (17) for LiCN, adopting the same four nonoverlapping π-pulses as above. This sequence corresponds to a switch in the molecular dipole from a large, negative value for S_0 to a large, positive value for S_2, followed by switching to the intermediate dipole of S_9, and, finally, all the way back. The time evolution of selected states is shown in Fig. 4, again for the "worst case" with $d=1a_0$.

From the figure we realize that the first pulse induces a population inversion from S_0 to S_2. Due to the high maximal intensity (9.12×10^{13} W/cm^2, see above), however, the inversion is incomplete. About 7% of the total population is lost by multiphoton excitation to ionizing states. The Keldysh[26] parameter is $\gamma\approx29$, so tunnel ionization plays an inferior role in this case. From Fig. 4 we further note that the second and third pulses do not cause significant further losses and the corresponding population inversions are nearly complete. This is a consequence of the fact that the second and third pulses are less intense (3.51×10^{10} W/cm^2, see above) and also less energetic ($\omega=0.0610E_h/\hbar$) than the first pulse, thus multiphoton transitions to ionizing above-threshold states are suppressed. Only when the fourth, high-intensity pulse comes in, an additional loss of about 6% is observed. The total loss of norm at the end of the pulse sequence is about 0.13 (which corresponds to the maximum in Fig. 2). At the end of the sequence, we find a population of 0.8640 in S_0, 0.0075 in S_2, and 0.0002 in S_9.

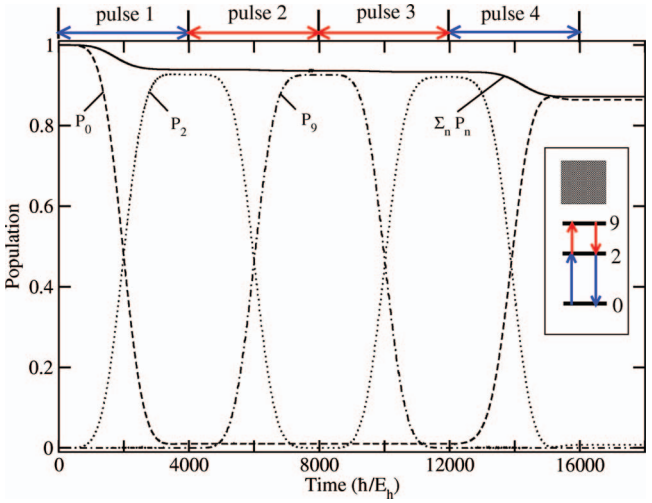

FIG. 4. Populations for the electronic ground state (P_0), the second (P_2), and the ninth excited state (P_9) of LiCN and the total norm ($\Sigma_n P_n$) during the π-pulse sequence (17). The double arrows indicate the pulse sequence and the inset shows schematically the excitation/deexcitation processes with the continuum indicated.

With $1/d$ set to zero, on the other hand, all ionization processes are suppressed and all transitions are almost fully state selective.[14] In this case the total norm is conserved and we end up with a population of 0.9866 in S_0, 0.0132 in S_2, and 0.0001 in S_9.

Despite population is lost by ionization when intense pulses are used, the switching process is still highly selective as desired. One can further improve selectivity by using longer, less intense pulses [cf. the π-pulse condition (16)], which reduces the amount of multiphoton ionization. Therefore, below-threshold excitation is typically not critically affected by ionization.

C. Transitions to ionizing states

This is, of course, radically different if "continuum" states above IP are the target states. Specifically, we choose the "resonance state" S_{69} at $E_{69}^{\mathrm{CIS}}=0.983\,49E_h$ with the comparatively low ionization rate of $\Gamma_{69}=4.45\times10^{-2}E_h/\hbar$ as outlined above. We adopt a two-pulse strategy, starting from S_0 with S_2 serving as an intermediate state, i.e.,

$$S_0\rightarrow S_2\rightarrow S_{69}, \tag{19}$$

because a direct excitation $S_0\rightarrow S_{69}$ is hampered by a prohibitively small transition dipole moment. In contrast, the transition dipole moment for excitation from S_2 to S_{69} is large, its dominant component being $\mu_{2,69,x}=-0.7255ea_0$. The first pulse enforcing the $S_0\rightarrow S_2$ transition is an x-polarized π-pulse with parameters $\sigma=4000\hbar/E_h$ (96.8 fs), $t_p=4000\hbar/E_h$ (96.8 fs), $\omega=0.2418E_h/\hbar$, and $f_0=0.0025E_h/ea_0$. The pulse is twice as long as the one in Sec. III B. Its maximal intensity is therefore reduced to 2.28×10^{13} W/cm^2 and multiphoton excitations are partially suppressed. Right after the first pulse, a second x-polarized π-pulse for the $S_2\rightarrow S_{69}$ transition is used with

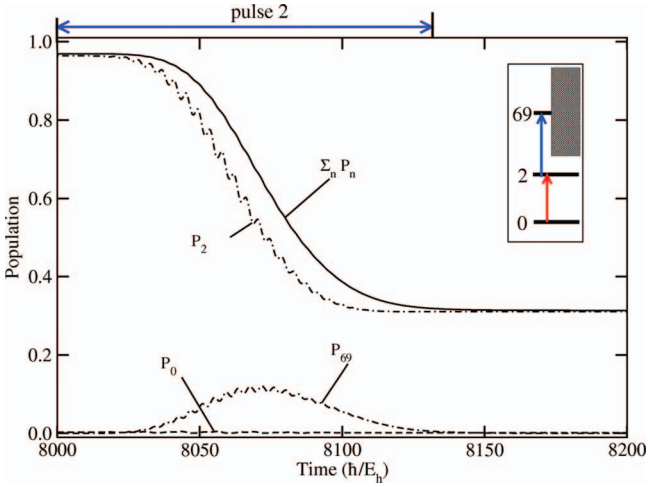

FIG. 5. Populations of relevant singlet states (P_0, P_2, P_{69}) and total norm $(\Sigma_n P_n)$ for a sequence with two π-pulses applied to LiCN. (The time evolution is shown after the first pulse only.)

$\omega=0.7417E_h/\hbar$, $\sigma=62.5\hbar/E_h$ (1.51 fs), $t_p=8062.5\hbar/E_h$ (195.0 fs), and $f_0=0.0693E_h/ea_0$. This corresponds to a maximal intensity of 1.68×10^{14} W/cm^2.

In Fig. 5, state populations of interest are shown for the time interval after the first pulse [i.e., for times $t>8000\hbar/E_h$ (193.5 fs)]. The first pulse leads to an almost complete $S_0\rightarrow S_2$ population inversion at $t=8000\hbar/E_h$ (193.5 fs) with only small losses due to the moderate pulse intensity, i.e., $P_2(8000)\approx0.97$. In contrast the transition $S_2\rightarrow S_{69}$ seems to be unselective, giving a maximal population of about 0.12 in the target state. The target state population decays on a femtosecond time scale due to the short lifetime of S_{69}. By this decay, and also by the even faster ionization of other "continuum states" which are also temporary populated, the total norm drops to about 0.31 at the end of the propagation.

Without ionization $(1/d=0)$, we obtain a final population in the S_{69} state of about 0.97 instead. Apart from S_0 and S_{69}, small populations in the order of about 0.006 are found in S_7, S_{72}, and S_{112}. All other states are only marginally populated at the end of the propagation. Thus, without ionization, the transitions are highly selective, otherwise ionization losses are the dominant effect.

IV. WAVE PACKET DYNAMICS AND PUMP-PROBE SPECTROSCOPY

The ionization losses can be used as a probe signal to monitor electron wave packet dynamics by pump-probe spectroscopy. An electronic wave packet can be created as a superposition of states below IP. In the following, we create, by a pump pulse, a superposition of states S_0 and S_9 of LiCN (see Fig. 1), which are connected by a large transition dipole moment of $\mu_{09,z}=-0.9580ea_0$. We use a z-polarized pump pulse with the following parameters: $\omega=0.3028E_h/\hbar$ $(=E_9^{\mathrm{CIS}}-E_0^{\mathrm{CIS}})$, $\sigma=1000\hbar/E_h$ (24.2 fs), $t_p=1000\hbar/E_h$ (24.2 fs), and $f_0=0.0011E_h/ea_0$. We thus have $|\mu_{09}||f_0|\sigma=0.335\pi$, which is not a π-pulse. Thus, not a pure state-to-state transition is enforced but a wave packet is created instead, which in good approximation is given by

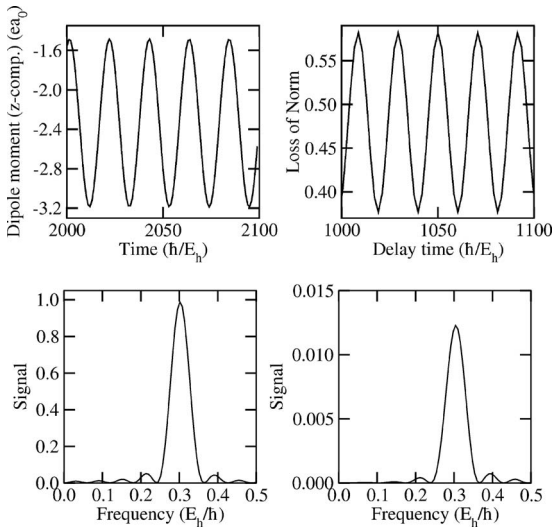

FIG. 6. Upper left panel: dipole moment $\mu_z(t)$ of LiCN in the interval $t\in[2000,2100]\hbar/E_h$ after a pump pulse was applied to create an electronic wave packet; lower left panel: Fourier transform of μ_z taken from the same interval. Upper right panel: "pump-probe spectrum" for delay times in the range $\Delta t_p\in[1000,1100]\hbar/E_h$; lower right panel: Fourier transform of pump-probe signal taken from the interval $[1000,1100]\hbar/E_h$.

$$\psi(t)=A_0e^{-iE_0t}|0\rangle+A_9e^{-iE_9t}|9\rangle \tag{20}$$

with $A_ne^{-iE_nt}=C_n(t)$. From an analytical solution of a two-level system in RWA, we estimate the population right after the probe pulse as $P_9=\sin^2(|\mu_{09}||f_0|\sigma/2)$, getting $P_9=|A_9^2|^2=|C_9|^2=0.25$, and $P_0=1-P_9=0.75$. In the actual simulation for the full system, we obtain $P_0=0.721$ and $P_9=0.273$, respectively. The wave packet gives rise to an oscillating dipole moment along z,

$$\mu_z(t)=A_0^2\mu_{00,z}+A_9^2\mu_{99,z}+2|A_0||A_9|\mu_{09,z}\cos(\omega_{90}t), \tag{21}$$

after the pump pulse is off. This is demonstrated in Fig. 6, which shows clear oscillations of μ_z in this regime. The initial rise in the dipole moment from $\mu_{00,z}=-3.708ea_0$ during the pump pulse up to $t=2000\hbar/E_h$ (48.4 fs) is not shown for clarity. The dipole oscillates around an average value of approximately $A_0^2\mu_{00,z}+A_9^2\mu_{99,z}=-2.34ea_0$ with an amplitude $2|A_0||A_9|\mu_{09,z}\approx0.85ea_0$. The ideal oscillation frequency is $\omega=\omega_{90}=0.3028E_h/\hbar$. This value is well reproduced by Fourier transforming $\mu_z(t)$ in the interval $t\in[2000,2100]\hbar/E_h$ $(t\in[48.4,50.8]$ fs), as shown in the lower left panel of Fig. 6. (The side wings are due to the finite transform interval.) The oscillation frequency corresponds to a period of $20.8\hbar/E_h$ or 0.5 fs.

We can probe the wave packet dynamics by a second probe pulse, which ionizes the molecule and which is delayed relative to the first one by a delay time Δt_p. Here we define Δt_p as the time span between the maxima of the pump [at $t_p=1000E_h/\hbar$ (24.2 fs)] and probe pulse. The probe pulse is x-polarized with the following parameters: $\omega=0.2500E_h/\hbar$, $\sigma=50\hbar/E_h$ $(\sim1.2$ fs), $t_p=1000\hbar/E_h+\Delta t_p$ (24.2 fs$+\Delta t_p$), and $f_0=0.0600E_h/ea_0$. The probe pulse is chosen short enough to resolve the oscillations of the wave packet. Not only by direct excitation but also by multiphoton excitation that parts of the wave packet are lifted to energies above IP. This causes a loss of norm. When computed after a

time $t=7000\hbar/E_h+\Delta t_p$ (169.3 fs$+\Delta t_p$), when the norm is constant, we obtain a highly oscillatory function. The latter is shown in Fig. 6, upper right panel, for a short interval $\Delta t_p \in [1000,1100]\hbar/E_h(\Delta t_p \in [24.2,26.6]$ fs). With the chosen parameters, the loss of norm oscillates around 50%. [The loss of norm was computed in a larger interval $\Delta t_p \in [-950,+1650]\hbar/E_h(\Delta t_p \in [-23.0,+39.9]$ fs), which is not shown here for clarity.] The oscillations in the pump-probe signal correspond to the oscillations with a frequency ω_{90} of the wave packet. This is again confirmed by Fourier transforming the signal from the time domain [in the interval $\Delta t_p \in [+1000,+1100]\hbar/E_h(\Delta t_p \in [24.2,26.6]$ fs)] to the frequency domain, as shown in the lower right panel of Fig. 6.

Note that a delay time $\Delta t_p=1000\hbar/E_h$ (24.2 fs) corresponds to the situation where the probe pulse is maximal at the moment when the probe pulse is over. At this time ($t=2000\hbar/E_h$(48.4 fs)), the dipole moment in Fig. 6, upper left panel, is close to its maximum. Half a period later, the wave packet shows a minimal dipole moment (or maximal negative dipole moment) with $\mu_z \approx -3.2ea_0$. The minimal dipole suggests a charge distribution similar to that of LiCN in the ionic ground state S_0, i.e., Li^+CN^-. In contrast, the maxima correspond to a case where the wave packet center moved in the direction toward the Li atom. According to Fig. 6, upper right panel, the maxima of the dipole moment correlate with the minima of the ionization probability, and vice versa. An interpretation is that ionization is easier when the electron wave packet is located closer to the cyano end of LiCN.

Of course, the suggested wave packet will be difficult to detect in a real experiment due to the short oscillation period and also due to the fact that nuclear motion cannot be neglected in LiCN where most excited states, including S_9, are dissociative. However, the technique may be successful for more rigid molecules.[40]

V. EFFECT ON POLARIZABILITIES

As a final example, we want to examine the performance of our simple model when applied to the calculation of electric response properties of molecules when stimulated by short laser pulses. For example, in Ref. 14, TD-CIS, TD-CIS(D), and TD-CISD were applied to determine the dynamic polarizability of H_2. Often, dynamic polarizabilities are calculated from the sum-over-states (SOS) method,[41] which is, however, perturbative. The approach of Ref. 14 is nonperturbative by solving Eq. (3) in the presence of a laser field $\underline{F}(t;\omega)$ given by Eqs. (14) and (15). From the induced dipole moment along direction $q(=x,y,z)$,

$$\mu_q^{\text{ind}}(t) = \alpha_{qq'}(-\omega,\omega)F_{q'}(t;\omega), \tag{22}$$

one obtains the elements of the dynamic polarizability tensor $\alpha_{qq'}(-\omega,\omega)$. This can also be done for arbitrarily shaped pulses, and the method can be extended to nonlinear response properties.[14] For the case without photoionization, according to the SOS formula the dynamic polarizability has a pole at a transition frequency to an excited state (if not a "dark" state).

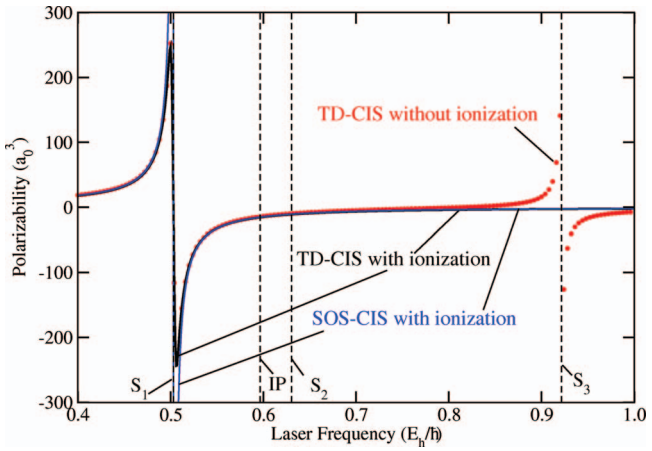

FIG. 7. Dynamic polarizability element $\alpha_{zz}(-\omega;\omega)$ for the hydrogen molecule using TD-CIS/cc-pVTZ without ionization (dots, red) and with ionization (solid line, black), as well as using SOS-CIS/cc-pVTZ (solid line, blue). The IP and the excitation energies from S_0 to S_1, S_2, and S_3 are shown as vertical, dashed lines.

In the present work we reinvestigate the H_2 molecule, however, in the presence of ionization. The TD-CIS method was used with a cc-pVTZ basis set[42] at a fixed H–H-bond length of $r_{\text{HH}}=1.393a_0$ (0.734 Å) obtained from RHF/cc-pVTZ geometry optimization. The CIS/cc-pVTZ calculation yields a first excited singlet state $S_1(^1\Sigma_u)$ at $E_1^{\text{CIS}}=0.503\,09E_h$ above the ground state $S_0(^1\Sigma_g)$. The next two singlet states are S_2 at $E_2^{\text{CIS}}=0.630\,47E_h$, which is dark, and S_3 at $E_3^{\text{CIS}}=0.921\,51E_h$ with a nonvanishing transition dipole moment $\mu_{03,z}$. The Koopmans' IP is $0.596\,44E_h$, i.e., states S_0 and S_1 are below and S_2 and S_3 are above IP. We adopted $\cos^2$ laser pulses, which are polarized along the molecular axis, with parameters $t_p=2000\hbar/E_h$ (48.4 fs), $\sigma=2000\hbar/E_h$ (48.4 fs), $f_{0,z}=0.005E_h/ea_0$, and variable carrier frequency ω. For the escape parameter d in Eq. (13), we chose $1/d=1a_0^{-1}$ (with photoionization) and $1/d=0$ (without photoionization), respectively. The polarizability element $\alpha_{zz}(-\omega,\omega)$ of the ground state S_0 was determined from Eq. (22).

In Fig. 7 we show the polarizability element $\alpha_{zz}(-\omega;\omega)$ for H_2 when calculated with various methods. The red bullets are for the ionization-free TD-CIS case. In this case one finds "quasipoles" at ω_{10} and ω_{30}. The latter is somewhat academic, since it is embedded in the ionization continuum. Around the excitation frequency ω_{20} the curve is flat because the transition dipole moment $\mu_{20,z}$ is zero. IP and the excitation energies are indicated in the figure as vertical lines. The situation changes drastically when ionization is included using our ionization model and TD-CIS (solid, black line). Now the S_3 "resonance" width is $\hbar\Gamma_3=0.786E_h$, corresponding to an extremely short "lifetime" of $1.27\hbar/E_h$ or 0.01 fs. In contrast, states below IP are stationary. As a consequence, the pole at $\omega=\omega_{30}$ is completely damped, rendering the α_{zz} curve flat in the region of ω_{30}. Other parts of the curve remain almost unaffected. In particular the quasisingularity around ω_{10} is unaffected. Finally, Fig. 7 shows as a blue, solid line the results of a SOS-CIS/cc-pVTZ calculation when generalized to finite lifetimes of excited states.[41] Accordingly, the real part of the polarizability tensor can be expressed, when adapted to our situation, as

$$\alpha^{R}_{qq'}(-\omega,\omega) = \sum_{n\neq 0}\left(\frac{\mu_{0n,q}\mu_{n0,q'}(\omega_{n0}-\omega)}{(\omega_{n0}-\omega)^2+\left(\frac{1}{2}\Gamma_n\right)^2} + \frac{\mu_{0n,q}\mu_{n0,q'}(\omega_{n0}+\omega)}{(\omega_{n0}+\omega)^2+\left(\frac{1}{2}\Gamma_n\right)^2}\right). \quad (23)$$

When using the SOS formula (23) with all the 29 excited singlet states obtained with TD-CIS/cc-pVTZ and the same lifetimes as in the TD-CIS calculation, we obtain the blue curve which closely resembles the one from TD-CIS/cc-pVTZ with ionization. There is a difference around ω_{10}, however, where Eq. (23) predicts a true pole, while our nonperturbative approach with finite pulse width gives a somewhat "damped" (or "quasi") pole instead.

To summarize this part, the ionization model suggested here seems to properly account for the above-threshold ionization effects during the electronic response of a molecule to laser pulses.

VI. CONCLUSIONS

In this paper, we developed a simple heuristic model for the above-threshold photoionization based on the TD-CI method. Accordingly, states above IP are assigned a certain width Γ_n, which can be interpreted as an absorbing potential, or inverse lifetime. All states below IP were treated as stationary. The widths Γ_n were estimated from a basic, classical ballistic model and an empirical decay length d. The latter was chosen in the present work to represent a "worst case scenario" with maximal ionization.

We showed for the example of dipole switching in the LiCN molecule that even in this scenario state-to-state transitions enforced by short π-pulses are not much affected by the above-threshold ionization. State-selective transitions are still possible as in the ionization free case.[14] Of course, when exciting into the (quasi) continuum above IP, ionization dominates. This ionization can be exploited to simulate pump-probe spectra of electronic wave packets created by ultrashort laser pulses. Finally, we have seen for the example of H_2 that the method may be used to calculate in a nonperturbative way the response properties of molecules stimulated by arbitrary laser pulses and under inclusion of ionization effects.

Of course, the present heuristic model has limitations which need to be overcome in the future. There is no information about the energy distribution of emitted electrons and no rescattering. Further, the parameter d is purely empirical. Finally, even states below IP may have a finite lifetime and are in general subject to energy and phase relaxation, in particular, when the molecule is embedded in an environment. These latter effects have been neglected in the present work but can be included using an open-system density matrix version of TD-CI as suggested elsewhere.[23] Also, especially in the case of molecules consisting of light atoms (such as H_2), nuclear dynamics may play a role on these time scales.

ACKNOWLEDGMENTS

This work was supported by Sonderforschungsbereich 450 of the Deutsche Forschungsgemeinschaft, *Analysis and Control of Ultrafast Photoinduced Processes* (subproject C7).

[1] M. Hentschel, R. Kienberger, C. Spielmann, N. Milosevic, T. Brabec, P. Corkum, U. Heinzmann, M. Drescher, and F. Krausz, Nature (London) **414**, 509 (2001).
[2] J. Itatani, H. Levesque, D. Zeidler, H. Niikura, H. Pépin, P. B. Corkum, and D. M. Villeneuve, Nature (London) **432**, 867 (2004).
[3] M. F. Kling, Ch. Siedschlag, A. J. Verhoef, J. I. Khan, M. Schultze, Th. Uphues, Y. Ni, M. Uiberacker, M. Drescher, F. Krausz, and M. J. Vrakking, Science **312**, 246 (2006).
[4] F. Krausz and M. Ivanov, Rev. Mod. Phys. **81**, 163 (2009).
[5] V. V. Vanne and A. Saenz, J. Phys. B **37**, 3973 (2005).
[6] G. K. Paramonov, Chem. Phys. Lett. **411**, 350 (2005).
[7] H. Kono, Y. Sato, M. Kanno, K. Nakai, and T. Kato, Bull. Chem. Soc. Jpn. **79**, 196 (2006).
[8] K. Burke, J. Werschnik, and E. K. U. Gross, J. Chem. Phys. **123**, 062206 (2005) (and references therein).
[9] A. Dreuw, J. L. Weisman, and M. Head-Gordon, J. Chem. Phys. **119**, 2943 (2003).
[10] T. Klamroth, Phys. Rev. B **68**, 245421 (2003) (and references therein).
[11] N. Rohringer, A. Gordon, and R. Santra, Phys. Rev. A **74**, 043420 (2006).
[12] H. B. Schlegel, S. Smith, and X. Li, J. Chem. Phys. **126**, 244110 (2007).
[13] P. Krause, T. Klamroth, and P. Saalfrank, J. Chem. Phys. **127**, 034107 (2007).
[14] P. Krause, T. Klamroth, and P. Saalfrank, J. Chem. Phys. **123**, 074105 (2005).
[15] F. Zanghellini, M. Kitzler, C. Fabian, T. Brabec, and A. Scrinzi, Laser Phys. **13**, 1064 (2003).
[16] T. Kato and H. Kono, Chem. Phys. Lett. **392**, 533 (2004).
[17] M. Nest, T. Klamroth, and P. Saalfrank, J. Chem. Phys. **122**, 124102 (2005).
[18] J. Breidbach and L. Cederbaum, J. Chem. Phys. **118**, 3983 (2003).
[19] I. Barth and J. Manz, Angew. Chem., Int. Ed. **45**, 2962 (2006).
[20] P. Krause and T. Klamroth, J. Chem. Phys. **128**, 234307 (2008).
[21] S. Klinkusch, T. Klamroth, and P. Saalfrank, Phys. Chem. Chem. Phys. **11**, 3875 (2009).
[22] T. Klamroth, J. Chem. Phys. **124**, 144310 (2006).
[23] J. C. Tremblay, T. Klamroth, and P. Saalfrank, J. Chem. Phys. **129**, 084302 (2008).
[24] C. Huber and T. Klamroth, Appl. Phys. A: Mater. Sci. Process. **81**, 91 (2004).
[25] P. Saalfrank, T. Klamroth, C. Huber, and P. Krause, Isr. J. Chem. **45**, 205 (2005).
[26] L. V. Keldysh, Zh. Eksp. Teor. Fiz. **47**, 1945 (1964); Sov. Phys. JETP **20**, 1307 (1965).
[27] A. M. Perelemov, V. S. Popov, and M. V. Terent'ev, Zh. Eksp. Teor. Fiz. **50**, 1393 (1966); Sov. Phys. JETP **23**, 924 (1966).
[28] M. V. Ammosov, N. B. Delone, and V. P. Krainov, Zh. Eksp. Teor. Fiz. **91**, 2008 (1986); Sov. Phys. JETP **64**, 1191 (1986).
[29] H.-D. Meyer, J. Chem. Phys. **105**, 1409 (1996).
[30] P. B. Corkum, Phys. Rev. Lett. **71**, 1994 (1993).
[31] M. Meckel, D. Comtois, D. Zeidler, A. Staudte, D. Pavicic, H. C. Badulet, H. Pepin, J. C. Kieffer, R. Dörner, D. M. Villeneuve, and P. B. Corkum, Science **320**, 1478 (2008).
[32] R. Paunz, *Spin Eigenfunctions* (Plenum, New York, 1979).
[33] L. Brillouin, Act. Sci. Ind. **71**, 159 (1933).
[34] M. Awasthi, Y. V. Vanne, and A. Saenz, J. Phys. B **38**, 3973 (2005).
[35] T. Koopmans, Physica (Amsterdam) **1**, 104 (1934).
[36] I. I. Rabi, Phys. Rev. **51**, 652 (1937).
[37] P. C. Hariharan and J. A. Pople, Theor. Chim. Acta **28**, 213 (1973).
[38] M. J. Frisch, G. W. Trucks, H. B. Schlegel *et al.*, GAUSSIAN03, Revision C.02, Gaussian, Inc., Wallingford, CT, 2004.
[39] M. W. Schmidt, K. K. Baldridge, J. A. Boatz, S. T. Elbert, M. S. Gordon, J. J. Jensen, S. Koseki, N. Matsunaga, K. A. Nguyen, S. J. Su, T. L. Windus, M. Dupuis, and J. A. Montgomery, J. Comput. Chem. **14**, 1347 (1993).
[40] S. Klinkusch and T. Klamroth (unpublished).
[41] L. Jensen, J. Autschbach, and G. C. Schatz, J. Chem. Phys. **122**, 224115 (2005).
[42] A. K. Wilson, T. van Mourik, and T. H. Dunning, J. Mol. Struct. **388**, 339 (1996).